Reflection Equivariant Quantum Neural Networks for Enhanced Image Classification

Maxwell West,[1, *] Martin Sevior,[1] and Muhammad Usman[1, 2, †]

[1]*School of Physics, The University of Melbourne, Parkville, 3010, VIC, Australia*
[2]*Data61, CSIRO, Clayton, 3168, VIC, Australia*

Machine learning is among the most widely anticipated use cases for near-term quantum computers, however there remain significant theoretical and implementation challenges impeding its scale up. In particular, there is an emerging body of work which suggests that generic, data agnostic quantum machine learning (QML) architectures may suffer from severe trainability issues, with the gradient of typical variational parameters vanishing exponentially in the number of qubits. Additionally, the high expressibility of QML models can lead to overfitting on training data and poor generalisation performance. A promising strategy to combat both of these difficulties is to construct models which explicitly respect the symmetries inherent in their data, so-called geometric quantum machine learning (GQML). In this work, we utilise the techniques of GQML for the task of image classification, building new QML models which are equivariant with respect to reflections of the images. We find that these networks are capable of consistently and significantly outperforming generic ansatze on complicated real-world image datasets, bringing high-resolution image classification via quantum computers closer to reality. Our work highlights a potential pathway for the future development and implementation of powerful QML models which directly exploit the symmetries of data.

1. Introduction

The significant interest in the possibility of realising superior machine learning algorithms on quantum computers has led over the last few years to intensive study of the capabilities and limitations of quantum machine learning (QML) models [1–10]. Although remarkable improvements in the capability of QML methods over their classical counterparts have been reported for some specific use cases [11–13], the extent to which they can be expected to perform well on general datasets remains an open question. In fact, recent work has suggested that generic, commonly employed QML architectures such as variational quantum circuits will face significant limitations due to their high expressibility and potentially low trainability resulting from barren plateaus in their training landscapes [14–19]. Efforts to address this, while still maintaining sufficiently complicated circuits to allow for the possibility of quantum advantage, are ongoing [18–22], but the ultimate resolution of the problem of barren plateaus remains unclear, and a key research direction of QML. Separately, in the case of image classification, the application of QML is still limited to relatively simple and low resolution datasets [23] by the current hardware limitations, with the development of high performance QML models for complex image datasets another important open problem. In this work we utilise techniques developed to tackle poor generalisation and barren plateaus to design new QML models which explicitly exploit the reflection symmetry inherent in many image datasets (see Figure 1). We establish that these reflection equivariant models can provide superior performance on complex images at the forefront of the current capabilities of QML, both obtaining higher accuracies and possessing parameter gradients which vanish more slowly than those of a generic counterpart.

Symmetry has long played an important role in physics,

facilitating both the discovery and understanding of the laws of nature [24]. More recently, the symmetries of data have been recognised to play an important role in machine learning, informing the design of some of the most effective classical classification algorithms [25]. Convolutional neural networks (CNNs), for example, which have been famously successful in the classification of image data, begin by applying a set of so-called convolutional filters, which act on all regions of the image identically – they have *translation equivariance* [26, 27]. The loss of expressibility that this necessarily entails has been found to be more than compensated for by their increased trainability, with CNNs having now dominated image classification for years [26, 28]. More generally, in recent years the new field of geometric deep learning (GDL) [25, 29–31] has begun to explore the role of symmetry respecting neural network architectures beyond such Euclidean translational equivariance, studying for example symmetries of data which lives on graphs [32] or Riemannian manifolds [33]. The observed success of these strategies naturally raises the question of whether such techniques could also help to build QML models which benefit from utilising the symmetries of their data.

Indeed, promising recent work has incorporated ideas from GDL into QML, resulting in the emerging subject of geometric quantum machine learning (GQML) [35–42]. For example, this approach has been used to construct QML models which, classifying data that enjoys permutation symmetry, provably avoid barren plateaus [38]. In this work we turn the techniques of GQML to the problem of image classification, an important example of a problem for which deep learning frameworks drastically outperform all other methods. The translational equivariance of CNNs has already been imported to the quantum setting, with quantum convolutional neural networks (QCNNs) offering a pathway to efficient image classification on quantum computers [8].
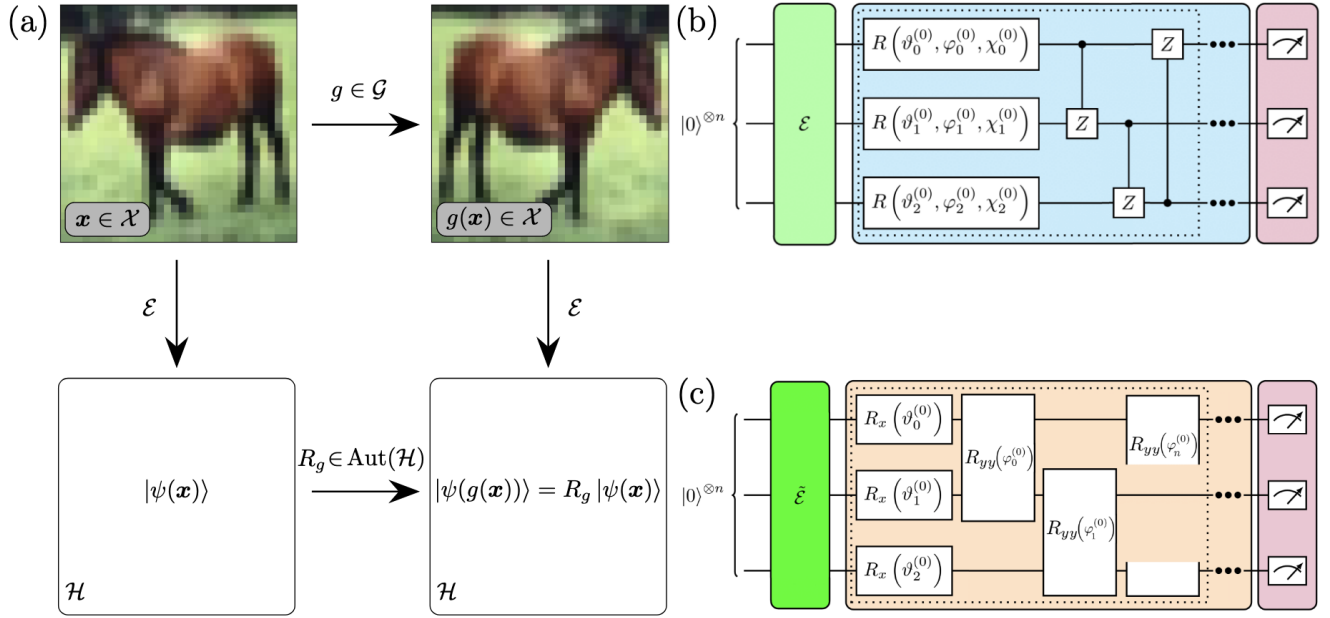
FIG. 1. **Reflection Equivariant Quantum Neural Networks.** (a) We consider image data whose labels are left invariant by the action of a group $\mathcal{G}$. In the case shown (from the CIFAR-10 dataset [34]), the label "horse" applies to the image both before and after a reflection about the central vertical axis. The action of the symmetry group on the encoded quantum states of the images is determined by a unitary representation R of $\mathcal{G}$ satisfying $|\psi(g(\boldsymbol{x}))\rangle = R_g |\psi(\boldsymbol{x})\rangle$ $\forall g \in \mathcal{G}, \boldsymbol{x} \in \mathcal{X}$, i.e. the diagram commutes. (b) A schematic depiction of the generic quantum variational classifier (QVC) that we employ for image classification. The pale green subcircuit $\mathcal{E}$ implements amplitude encoding. The variational component of the circuit consists of the unit in the dotted box repeated 100 times (with different parameters in each layer). Finally, σ_z measurements are made on each qubit to determine the label prediction. (c) A modified circuit which possesses reflection equivariance. The encoding subcircuit $\tilde{\mathcal{E}}$ now includes an additional change of basis following the amplitude encoding (see the text and Figure 3). In the variational section, which again consists of the unit in the dotted box repeated 100 times, gates which commute wth the symmetry operations are chosen. Finally, σ_z measurements are again made to determine the label prediction, although this time products of the measurement outcomes on neighbouring qubits are used in order to retain equivariance (see the text). While (b) and (c) depict 3-qubit cartoons of the two models, the actual circuits employ either 10 or 12 qubits depending on the dataset due to the resolution of the images: $1{\times}28{\times}28$ for MNIST, and $3{\times}32{\times}32$ for CIFAR-10 and CelebA (see Figure 2).

Here we consider the alternative symmetry of reflections, noting that the labels assigned to an image will often be independent of reflections of that image about various axes (see Figure 1(a)), as for example in most common object identification problems. We construct reflection equivariant quantum neural networks (REQNNs, see Figure 1(c)) and show that they consistently outperform a generic model (see Figure 1(b)) when benchmarked across three standard image datasets (CIFAR-10 [34], MNIST [26], and Celeb-A [43] – see Figure 2 for examples of images from each dataset), despite having access to fewer trainable parameters. These results provide concrete evidence supporting the emerging philosophy that sacrificing generality and expressibility in favour of targeting a smaller but more meaningful fraction of the model space is a promising approach forward for QML. Moreover, by demonstrating enhanced performance for image classification through the use of reflection equivariant networks, separate to the previous use of a translation equivariant convolutional structure in QCNNs [8], our results encourage the future development of QML models which exploit as much of the available symmetry information of their data as possible, including extensions to additional symmetries and the simultaneous consideration of multiple symmetries. The practical realisation of tailored QML models such as these will bring the possibility of successfully applying quantum computing to the many domains of ML, both image-based and otherwise, closer to reality.

2. Geometric Quantum Machine Learning

We begin by briefly summarising the aspects of GQML relevant to our construction of REQNNs, introducing the notation and formalism required to discuss equivariance and symmetry operations on data encoded into quantum states. Interested readers can find further details of GQML in Refs. [36, 37]. We consider the classification of (image) data $\boldsymbol{x} \in \mathcal{X}$, with associated labels $y(\boldsymbol{x}) \in \mathcal{Y}$. Our QML models will follow a standard three-step procedure: a data encoding circuit which maps the classical image data $\boldsymbol{x}$ to a quantum state, $\boldsymbol{x} \mapsto |\psi(\boldsymbol{x})\rangle$, followed by a variational circuit U_θ, followed by measurements of a set of operators $\{M_j\}_{j=1}^{n_{\text{classes}}}$ to determine the class label. For a given set of parameters $\theta \in \Theta$ the prediction $\hat{y}_\theta(\boldsymbol{x})$ of the model on an input $\boldsymbol{x}$ is given by

$$\hat{y}_\theta(\boldsymbol{x}) = \underset{j}{\operatorname{argmax}} \langle \psi(\boldsymbol{x})| \mathcal{U}_\theta^\dagger M_j \mathcal{U}_\theta |\psi(\boldsymbol{x})\rangle \tag{1}$$

We also introduce a symmetry group $\mathcal{G}$ which we will identify with its action on $\mathcal{X}$, i.e. writing $\mathcal{G} : \mathcal{X} \to \mathcal{X}$, with $g(\boldsymbol{x})$ for $g \in \mathcal{G}$ the image obtained by performing the symmetry

transformation g on $\boldsymbol{x}$. We emphasise that the symmetries are expected to be respected only at the level of the labels of the data, i.e. $y(g(\boldsymbol{x})) = y(\boldsymbol{x}) \; \forall \boldsymbol{x} \in \mathcal{X}, \; g \in \mathcal{G}$, but perhaps $g(\boldsymbol{x}) \neq \boldsymbol{x}$. In this work we will focus on the group which enacts reflections about the central vertical axis of the images, so that $\mathcal{G} \cong \mathbb{Z}_2$. The group will act on the Hilbert space $\mathcal{H}$ of the quantum computer via a unitary representation $R : \mathcal{G} \to \mathrm{Aut}(\mathcal{H})$ which satisfies $R(g) |\psi(\boldsymbol{x})\rangle = |\psi(g(\boldsymbol{x}))\rangle$. Henceforth we write $R_g \equiv R(g)$. We wish for the predictions of our QNN to be $\mathcal{G}$-invariant, i.e.

$$\hat{y}_\theta(\boldsymbol{x}) = \hat{y}_\theta(g(\boldsymbol{x})) \qquad \forall g \in \mathcal{G}, \boldsymbol{x} \in \mathcal{X}, \theta \in \Theta \qquad (2)$$

From Equation 1 we have that

$$\hat{y}_\theta(g(\boldsymbol{x})) = \mathrm{argmax}_j \langle \psi(g(\boldsymbol{x})) | \mathcal{U}_\theta^\dagger M_j \mathcal{U}_\theta | \psi(g(\boldsymbol{x})) \rangle \qquad (3)$$

$$= \mathrm{argmax}_j \langle \psi(\boldsymbol{x}) | R_g^\dagger \mathcal{U}_\theta^\dagger M_j \mathcal{U}_\theta R_g | \psi(\boldsymbol{x}) \rangle \qquad (4)$$

and therefore the condition of Equation 2 will be satisfied if

$$\left[R_g, \; \mathcal{U}_\theta^\dagger M_j \mathcal{U}_\theta \right] = 0 \qquad \forall g \in \mathcal{G}, \boldsymbol{x} \in \mathcal{X}, \theta \in \Theta \qquad (5)$$

We refer to QNNs satisfying this condition as reflection equivariant.

3. Results

Our first task in building REQNNs is to establish the unitary representation of the symmetry group $\mathcal{G}$. As in our case $\mathcal{G} \cong \mathbb{Z}_2$, there is only one nontrivial symmetry operator R_g, namely the one which maps a state to the state encoding the reflection of the image encoded by the original state. As we have $R_g |\psi(\boldsymbol{x})\rangle = |\psi(g(\boldsymbol{x}))\rangle$ for all images $\boldsymbol{x}$, R_g will be determined by the form of the data encoding map, to which we now turn. Due to our desire to classify high dimensional image data using only the relatively small number of qubits available to classical simulators we need to employ a method of encoding which is highly efficient in the number of qubits required. For this reason we choose amplitude encoding, i.e., if $\boldsymbol{x}$ is a vector containing the pixel values of an image then we construct the state

$$\boldsymbol{x} \mapsto |\psi(\boldsymbol{x})\rangle = \sum_i x_i |i\rangle$$

As there are 2^n amplitudes available for an n qubit state, only $\lceil \log_2(CLW) \rceil$ qubits are needed, where C is the number of channels of the image, L is the length, and W the width. For MNIST, we have $(C, L, W) = (1, 28, 28)$ and therefore require 10 qubits, and for CIFAR-10 and CelebA $(C, L, W) = (3, 32, 32)$, requiring 12. In both cases we append and prepend zeros equally in order to obtain an input vector of length a power of two in order to proceed with the amplitude encoding.

Unfortunately, standard amplitude encoding will render R_g a complicated, non-local operator which will be difficult to work with in practice, especially on real hardware with constrained qubit connectivity. In order to rectify this we

FIG. 2. **Image datasets.** We consider three standard image datasets from the ML literature: MNIST [26], CIFAR-10 [34] and CelebA [43]. The MNIST dataset consists of handwritten digits, CIFAR-10 of various objects and animals, and CelebA of human faces. In the case of MNIST we restrict our attention to the digits "0", "1" and "8". Having done this, all of the data we consider has labels which are unchanged under a horizontal reflection and is therefore suitable for classification by our REQNNs.

FIG. 3. **Amplitude Encoding.** Encoding for an example 4×4 image. The pixels are numbered by the index of the basis state into the amplitude of which they are encoded. (a) The standard case. For example, the pixel value of the pixel in the top right corner is encoded into the amplitude of $|3\rangle \equiv |0011\rangle$. (b) Here we permute the order of the encoding. For example, the pixel value of the pixel in the top right corner is now encoded into the amplitude of $|15\rangle \equiv |1111\rangle$. In this case a horizontal reflection is represented by $X^{\otimes n}$.

consider, for our equivariant models, a slight modification of standard amplitude encoding which entails rearranging the order in which the pixel values are encoded so as to produce an encoding with respect to which we have $R_g = X^{\otimes n}$ (see Figure 3). The standard order in which the pixel values are read is shown in Figure 3(a) for an example of a 4×4 greyscale (i.e. only one channel) image, and our alternate encoding in Figure 3(b). The encoding strategy of Figure 3(a) is employed in the generic model (Figure 1(b)), and the strategy of Figure 3(b) in the equivariant model (Figure 1(c) of the main text). In the second case, a reflection of the image is represented at the Hilbert space level by
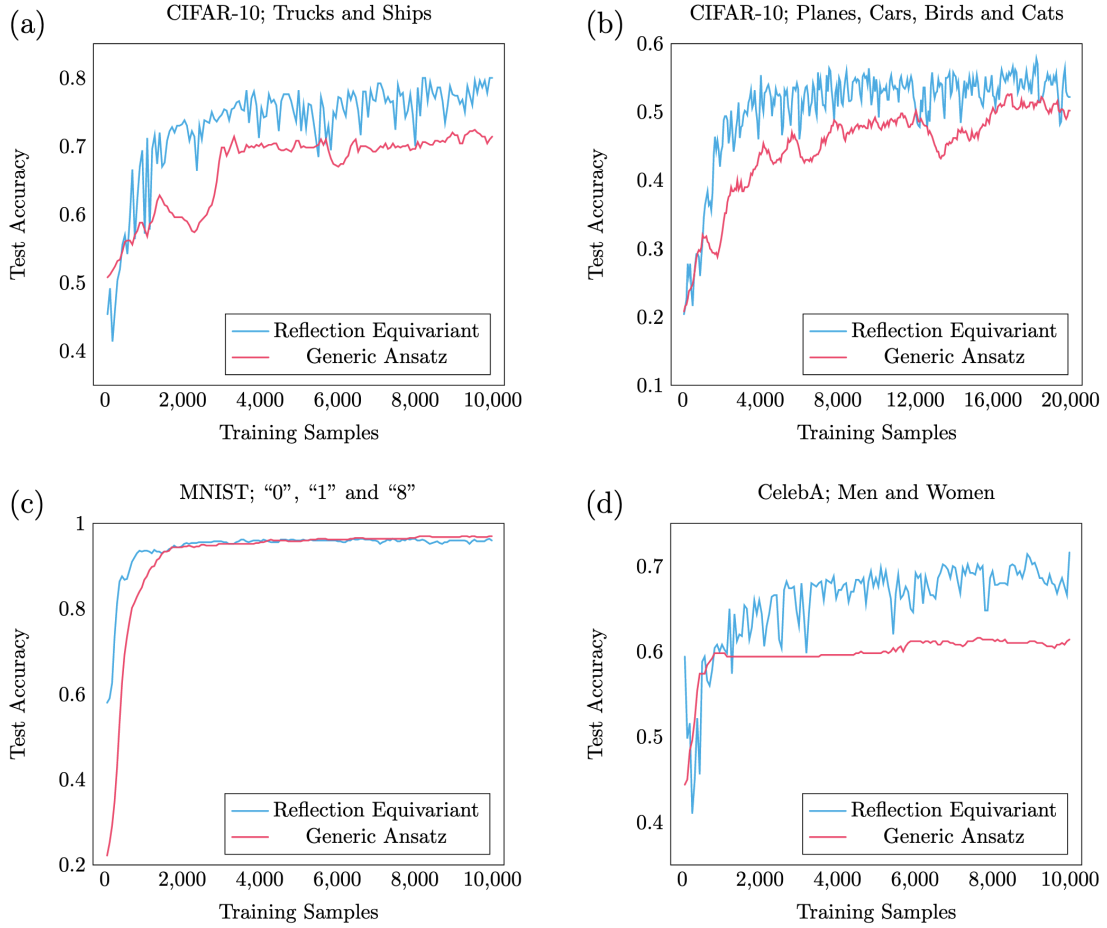
FIG. 4. **Quantum neural network performances.** We compare the performance of the generic and reflection equivariant QNNs across a range of image datasets. As the different datasets have varying resolutions, the number of qubits needed to implement the models also changes (see the Results section), providing another axis along which to contrast the performance of the two classes of models. We find that the reflection equivariant QNNs learn more quickly than their generic counterparts consistently across different datasets, number of classes, and number of qubits used to implement the QNNs. The plotted accuracies refer to 500 test samples, calculated at various points throughout the training process. (a, b) Two and four class classification using the CIFAR-10 dataset, respectively. (c) Three class classification with the MNIST dataset. Although this dataset is quite simple, and QNNs have previously been used to achieve high accuracy on all ten classes [13], we restrict here to the digits "0", "1" and "8" as they are the only ones which (approximately) respect the reflection symmetry. Both models achieve high test accuracy (>96%), but the reflection equivariant model learns more quickly. (d) The CelebA dataset consists of images of human faces. We consider the classification task of determining the gender of the imaged person, again finding that the reflection equivariant model significantly outperforms its generic counterpart.

the operator $X^{\otimes n}$, which exchanges the basis states $|i\rangle$ and $|2n - 1 - i\rangle$. The case of three channel RGB images is similar, with the order that the data is encoded chosen so as to enforce the requirement that, for every pixel and every channel, the amplitude of the states $|i\rangle$ and $|2n - 1 - i\rangle$ are the values (in a given channel) of a pair of pixels related by the vertical reflection. With this choice of encoding we have that $R_g |\psi(\boldsymbol{x})\rangle = |\psi(g(\boldsymbol{x}))\rangle$ for $g = e, r$ the identity and horizontal reflection operations on the images respectively, with $R_e = I$, $R_r = X^{\otimes n}$. Armed with the representation of our symmetry group (consisting simply of the operators $\{I, X^{\otimes n}\}$) we are ready to begin constructing REQNNs.

Given a symmetry group $\mathcal{G}$ and a unitary representation R, various ways of constructing equivariant QNNs have been proposed. Ref. [35], for example, takes a standard set of gates and "symmetrises" them, building new gates which are guaranteed to commute with the symmetry representation.

Here, benefiting from the simplicity of our representation, we adopt a different approach, simply manually selecting gates and measurements which commute with $X^{\otimes n}$ and therefore satisfy Equation 5. Schematic depictions of the two models considered in this work are shown in Figure 1(b,c). The model of Figure 1(b) is a "generic ansatz" consisting of amplitude encoding followed by a standard variational circuit followed by σ_z measurements on the first n_{classes} qubits. The prediction of the model is taken to be the class corresponding to the qubit which reports the largest such measurement (i.e. $M_j = \sigma_z^{(j)}$ in the notation of Equation 1, with $\sigma_z^{(j)}$ the Pauli z operator acting on the jth qubit). The reflection equivariant model of Figure 1(c) differs in several ways. First, the encoding stage is slightly modified as previously discussed (see also Figure 3). Second, the variational component is built from R_x and R_{yy} gates, both of which commute with $X^{\otimes n}$. Finally, the class labels are

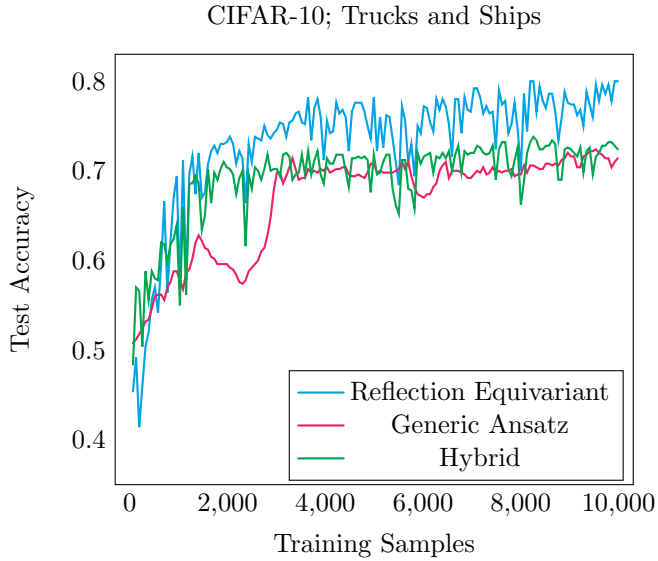CIFAR-10; Trucks and Ships

Parameter Gradient Variance

FIG. 5. **Effect of reflection equivariance.** In addition to the considered generic and reflection equivariant models we trial a "hybrid" model with the same variational circuit structure and final measurement strategy as the reflection equivariant model, but which uses the standard amplitude encoding map $\mathcal{E}$ (Figure 3 (a)) instead of the modified map $\tilde{\mathcal{E}}$ (Figure 3 (b)). Therefore, the hybrid model continues to commute with $X^{\otimes n}$, but this operator no longer represents a meaningful transformation of the data. The considerable drop in accuracy from the reflection equivariant model, despite sharing the same variational architecture, confirms the importance of respecting meaningful symmetries of the data.
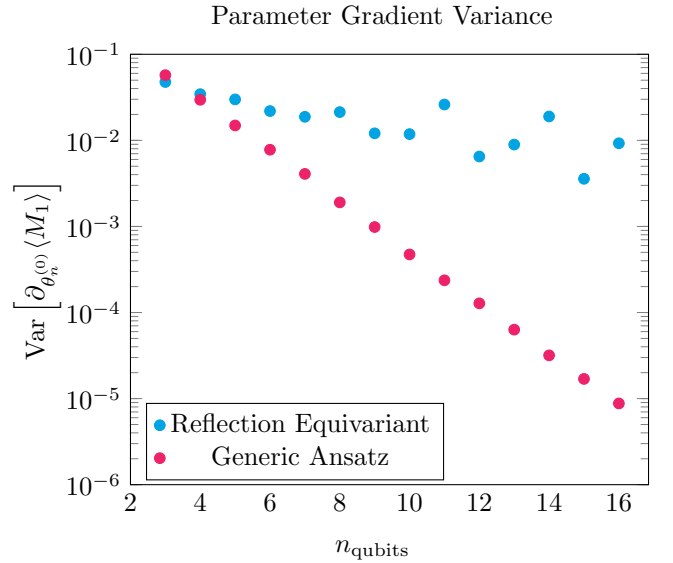
FIG. 6. **Variance of parameter gradients.** We calculate the derivative of the expectation value of the measured operator M_1 in both the generic and reflection equivariant cases with respect to the first variational parameter in the final layer of the circuits. This is repeated for 3000 random circuit initialisations, and the variance of the results is plotted as a function of the number of qubits. At the number of qubits relevant for this work ($n_{\mathrm{qubits}} = 10, 12$) we find that the variance of the gradients in the equivariant case is several orders of magnitude higher than the generic case. This is consistent with the improved trainability observed for the equivariant networks, as well as the increased volatility of the test accuracies seen in Figures 4 and 5.

determined by measurements $M_j = \sigma_z^{(j)} \otimes \sigma_z^{(j+1 \bmod n)}$, which also commute with $X^{\otimes n}$. This QNN therefore satisfies the equivariance condition of Equation 5.

We implement the networks within the Pennylane framework [44], and train them using the Nesterov momentum optimiser [45]. The results are shown in Figure 4. Our results show that the reflection equivariant model consistently outperforms the generic model, despite its lower expressibility and the generic model containing 50% more trainable parameters. The increased performance is particularly notable in the cases of the more complicated datasets, CIFAR-10 and Celeb-A, which consist of colour (RGB) images. In the case of MNIST, and although the difference in final test accuracies is negligible, we nonetheless see the reflection equivariant model learning more quickly in the initial stage of training, with its focus narrowed to the more meaningful subset of reflection insensitive decision functions.

As the reflection equivariant and generic classifiers considered in this work are constructed from substantially different quantum circuits, there is a possibility that the enhanced performance of the reflection equivariant model is due to some other factor than its respecting of the symmetry. In order to separate the effect of simply moving to a different circuit architecture from the role played by the reflection equivariance we consider a "hybrid" model consisting of the standard encoding $\mathcal{E}$ of Figure 1(b) (see also Figure 3(a)), and the variational body and measurements of Figure 1(c). This

produces a model with the same restricted expressibility of the reflection equivariant model, which remains equivariant with respect to the operator $X^{\otimes n}$, but for which $X^{\otimes n}$ no longer enacts a meaningful symmetry. The results, shown in Figure 5, show the reflection equivariant model significantly outperforming this hybrid model, confirming the importance of building networks which respect genuine symmetries of the data.

Being represented by a group with only two elements, we do not expect the respecting of reflection symmetry to lead to a provable avoidance of barren plateaus as has been previously reported in the case of permutation symmetry [38], but our results here are an encouraging sign that, even in the absence of such guarantees, considerable gains in accuracy may be realised by such models in practice. To explore this further we numerically investigate the variance of the gradient of a measured Pauli observable in both the generic and reflection equivariant cases (see Figure 6, c.f. Figure 3 of Ref. [14]). As expected, the (universal) generic model experiences a barren plateau, with exponentially vanishing gradients. While we also see approximately exponential decreases in the (non-universal) reflection equivariant model, the rate of decrease is drastically reduced, indicating that training will remain feasible for much larger quantum circuits. This is consistent with our expectation that, while the REQNNs may also asymptotically experience barren plateaus, they will be able to offer enhanced performance in the highly

interesting region of several tens of qubits explored in this work and accessible on near-term hardware.

4. Conclusion

Geometric quantum machine learning is rapidly emerging as a promising research direction which may ameliorate two of the key challenges facing QML: barren plateaus and overfitting. We have applied the techniques of GQML to the task of creating QML models for image classification which are equivariant with respect to horizontal reflections, finding a consistent improvement over generic, symmetry agnostic models, despite those models being more expressive. These encouraging results join the previous GQML literature [35–42] in demonstrating clear advantages in building tailored QML models which respect the symmetry of the data they are attempting to classify, rather than simply employing universal models, and provide further evidence of the potential of this research direction in the NISQ era and beyond.

References

* westm2@student.unimelb.edu.au
† musman@unimelb.edu.au

[1] J. Biamonte, P. Wittek, N. Pancotti, P. Rebentrost, N. Wiebe, and S. Lloyd, "Quantum machine learning," *Nature*, vol. 549, no. 7671, pp. 195–202, 2017.

[2] K. Beer, D. Bondarenko, T. Farrelly, T. J. Osborne, R. Salzmann, D. Scheiermann, and R. Wolf, "Training deep quantum neural networks," *Nature Communications*, vol. 11, no. 1, pp. 1–6, 2020.

[3] V. Havlíček, A. D. Córcoles, K. Temme, A. W. Harrow, A. Kandala, J. M. Chow, and J. M. Gambetta, "Supervised learning with quantum-enhanced feature spaces," *Nature*, vol. 567, no. 7747, pp. 209–212, 2019.

[4] J. Romero, J. P. Olson, and A. Aspuru-Guzik, "Quantum autoencoders for efficient compression of quantum data," *Quantum Science and Technology*, vol. 2, no. 4, p. 045001, 2017.

[5] P.-L. Dallaire-Demers and N. Killoran, "Quantum generative adversarial networks," *Physical Review A*, vol. 98, no. 1, p. 012324, 2018.

[6] N. Killoran, T. R. Bromley, J. M. Arrazola, M. Schuld, N. Quesada, and S. Lloyd, "Continuous-variable quantum neural networks," *Physical Review Research*, vol. 1, no. 3, p. 033063, 2019.

[7] M. Schuld and N. Killoran, "Quantum machine learning in feature hilbert spaces," *Physical review letters*, vol. 122, no. 4, p. 040504, 2019.

[8] I. Cong, S. Choi, and M. D. Lukin, "Quantum convolutional neural networks," *Nature Physics*, vol. 15, no. 12, pp. 1273–1278, 2019.

[9] M. Schuld, "Supervised quantum machine learning models are kernel methods," *arXiv preprint arXiv:2101.11020*, 2021.

[10] S. L. Tsang, M. T. West, S. M. Erfani, and M. Usman, "Hybrid quantum-classical generative adversarial network for high resolution image generation," *arXiv preprint arXiv:2212.11614*, 2022.

[11] Y. Liu, S. Arunachalam, and K. Temme, "A rigorous and robust quantum speed-up in supervised machine learning," *Nature Physics*, vol. 17, no. 9, pp. 1013–1017, 2021.

[12] H.-Y. Huang, M. Broughton, J. Cotler, S. Chen, J. Li, M. Mohseni, H. Neven, R. Babbush, R. Kueng, J. Preskill *et al.*, "Quantum advantage in learning from experiments," *Science*, vol. 376, no. 6598, pp. 1182–1186, 2022.

[13] M. T. West, S. M. Erfani, C. Leckie, M. Sevior, L. C. Hollenberg, and M. Usman, "Benchmarking adversarially robust quantum machine learning at scale," *arXiv preprint arXiv:2211.12681*, 2022.

[14] J. R. McClean, S. Boixo, V. N. Smelyanskiy, R. Babbush, and H. Neven, "Barren plateaus in quantum neural network training landscapes," *Nature Communications*, vol. 9, no. 1, pp. 1–6, 2018.

[15] Z. Holmes, K. Sharma, M. Cerezo, and P. J. Coles, "Connecting ansatz expressibility to gradient magnitudes and barren plateaus," *PRX Quantum*, vol. 3, no. 1, p. 010313, 2022.

[16] M. Cerezo, A. Sone, T. Volkoff, L. Cincio, and P. J. Coles, "Cost function dependent barren plateaus in shallow parametrized quantum circuits," *Nature Communications*, vol. 12, no. 1, pp. 1–12, 2021.

[17] S. Wang, E. Fontana, M. Cerezo, K. Sharma, A. Sone, L. Cincio, and P. J. Coles, "Noise-induced barren plateaus in variational quantum algorithms," *Nature Communications*, vol. 12, no. 1, pp. 1–11, 2021.

[18] A. Pesah, M. Cerezo, S. Wang, T. Volkoff, A. T. Sornborger, and P. J. Coles, "Absence of barren plateaus in quantum convolutional neural networks," *Physical Review X*, vol. 11, no. 4, p. 041011, 2021.

[19] T. L. Patti, K. Najafi, X. Gao, and S. F. Yelin, "Entanglement devised barren plateau mitigation," *Physical Review Research*, vol. 3, no. 3, p. 033090, 2021.

[20] A. Skolik, J. R. McClean, M. Mohseni, P. van der Smagt, and M. Leib, "Layerwise learning for quantum neural networks," *Quantum Machine Intelligence*, vol. 3, no. 1, pp. 1–11, 2021.

[21] T. Volkoff and P. J. Coles, "Large gradients via correlation in random parameterized quantum circuits," *Quantum Science and Technology*, vol. 6, no. 2, p. 025008, 2021.

[22] E. Grant, L. Wossnig, M. Ostaszewski, and M. Benedetti, "An initialization strategy for addressing barren plateaus in parametrized quantum circuits," *Quantum*, vol. 3, p. 214, 2019.

[23] S. Lu, L.-M. Duan, and D.-L. Deng, "Quantum adversarial machine learning," *Physical Review Research*, vol. 2, no. 3, p. 033212, 2020.

[24] E. Noether, "Invariante variationsprobleme," *Nachrichten von der Gesellschaft der Wissenschaften zu Göttingen, Mathematisch-Physikalische Klasse*, vol. 1918, pp. 235–257, 1918. [Online]. Available: http://eudml.org/doc/59024

[25] T. S. Cohen *et al.*, "Equivariant convolutional networks," 2021.

[26] Y. Lecun, L. Bottou, Y. Bengio, and P. Haffner, "Gradient-based learning applied to document recognition," *Proceedings of the IEEE*, vol. 86, no. 11, pp. 2278–2324, 1998.

[27] R. Kondor and S. Trivedi, "On the generalization of equivariance and convolution in neural networks to the action of compact groups," in *International Conference on Machine Learning*. PMLR, 2018, pp. 2747–2755.

[28] K. He, X. Zhang, S. Ren, and J. Sun, "Deep residual learning for image recognition," in *Proceedings of the IEEE conference on computer vision and pattern recognition*, 2016, pp. 770–778.

[29] M. M. Bronstein, J. Bruna, Y. LeCun, A. Szlam, and P. Vandergheynst, "Geometric deep learning: Going beyond eu-

clidean data," *IEEE Signal Processing Magazine*, vol. 34, no. 4, pp. 18–42, 2017.

[30] M. M. Bronstein, J. Bruna, T. Cohen, and P. Veličković, "Geometric deep learning: Grids, groups, graphs, geodesics, and gauges," *arXiv preprint arXiv:2104.13478*, 2021.

[31] Z. Li, H. Zheng, E. Thiede, J. Liu, and R. Kondor, "Group-equivariant neural networks with fusion diagrams," *arXiv preprint arXiv:2211.07482*, 2022.

[32] B. Perozzi, R. Al-Rfou, and S. Skiena, "Deepwalk: Online learning of social representations," in *Proceedings of the 20th ACM SIGKDD international conference on Knowledge discovery and data mining*, 2014, pp. 701–710.

[33] J. Masci, D. Boscaini, M. Bronstein, and P. Vandergheynst, "Geodesic convolutional neural networks on riemannian manifolds," in *Proceedings of the IEEE international conference on computer vision workshops*, 2015, pp. 37–45.

[34] A. Krizhevsky, G. Hinton *et al.*, "Learning multiple layers of features from tiny images," 2009.

[35] J. J. Meyer, M. Mularski, E. Gil-Fuster, A. A. Mele, F. Arzani, A. Wilms, and J. Eisert, "Exploiting symmetry in variational quantum machine learning," *arXiv preprint arXiv:2205.06217*, 2022.

[36] M. Ragone, P. Braccia, Q. T. Nguyen, L. Schatzki, P. J. Coles, F. Sauvage, M. Larocca, and M. Cerezo, "Representation theory for geometric quantum machine learning," *arXiv preprint arXiv:2210.07980*, 2022.

[37] Q. T. Nguyen, L. Schatzki, P. Braccia, M. Ragone, P. J. Coles, F. Sauvage, M. Larocca, and M. Cerezo, "Theory for equivariant quantum neural networks," *arXiv preprint arXiv:2210.08566*, 2022.

[38] L. Schatzki, M. Larocca, F. Sauvage, and M. Cerezo, "Theoretical guarantees for permutation-equivariant quantum neural networks," *arXiv preprint arXiv:2210.09974*, 2022.

[39] F. Sauvage, M. Larocca, P. J. Coles, and M. Cerezo, "Building spatial symmetries into parameterized quantum circuits for faster training," *arXiv preprint arXiv:2207.14413*, 2022.

[40] A. Skolik, M. Cattelan, S. Yarkoni, T. Bäck, and V. Dunjko, "Equivariant quantum circuits for learning on weighted graphs," *arXiv preprint arXiv:2205.06109*, 2022.

[41] M. Larocca, F. Sauvage, F. M. Sbahi, G. Verdon, P. J. Coles, and M. Cerezo, "Group-invariant quantum machine learning," *arXiv preprint arXiv:2205.02261*, 2022.

[42] H. Zheng, G. S. Ravi, H. Wang, K. Setia, F. T. Chong, and J. Liu, "Benchmarking variational quantum circuits with permutation symmetry," *arXiv preprint arXiv:2211.12711*, 2022.

[43] S. Yang, P. Luo, C.-C. Loy, and X. Tang, "From facial parts responses to face detection: A deep learning approach," in *Proceedings of the IEEE international conference on computer vision*, 2015, pp. 3676–3684.

[44] V. Bergholm, J. Izaac, M. Schuld, C. Gogolin, M. S. Alam, S. Ahmed, J. M. Arrazola, C. Blank, A. Delgado, S. Jahangiri *et al.*, "Pennylane: Automatic differentiation of hybrid quantum-classical computations," *arXiv preprint arXiv:1811.04968*, 2018.

[45] Y. Nesterov, "A method for solving the convex programming problem with convergence rate $o(1/k^2)$," *Proceedings of the USSR Academy of Sciences*, vol. 269, pp. 543–547, 1983.